

Solar variation and Super Geomagnetic Storm Event of solar cycle 24 during period from 10 March to 31 March 2015

¹Udayveer Vikram Singh Bundela , ²Dr. Sushil Kumar Sharma,

³Dr. C.M.Tiwari

¹udayraja495@gmail.com

Research center- Govt.PG(Auto.) Satna (M.P.)

²Govt. PG college, Satna (M.P.)

Email - bcs.sks@gmail.com

³Email- cmtiwari_2005@yahoo.com

Abstract:

Important solar ejections that generate storms in the heliosphere include CMEs and solar flares. The Earth's magnetic field is changing as a result of these ejections. In this article, we examine the solar cycle 24 heliospheric disruption that occurred between March 10 and March 31, 2015. We noted that on March 15, 2015, a massive burst of magnetic field and plasma from the Sun's corona, together with related solar flares, altered space weather towards Earth and resulted in the largest geomagnetic storm on March 17. We discovered that on March 17, 2015, the Dst value dropped to a minimum of -223 nT and an FDs. Notably, the storm had two steps. It is possible to link the solar event to the storm's origin. on March 15, 2015. On that day, at 2:10 UT, the SOHO/LASCO C3 spacecraft detected a partial halo coronal mass ejection (CME) that was connected to a C9.1/1F flare (S22W25) and a string of type II/IV radio bursts. This CME's initial propagation speed is predicted to be around 668 km/s. On March 17, at 3:59 UT, an interplanetary (IP) shock that was probably fueled by a magnetic cloud (MC) reached the Wind spacecraft and immediately began a storm. After the It is discovered that the first phase is the result of the MC passing through the southbound IMF component. The only solar source of the MC is the CME that erupted on March 15. In-depth information from measurements (Wind and SOHO) and our algorithm (Dstmin) for forecasting the strength

Keywords: Coronal mass ejection, interplanetary shock, Super geomagnetic storm, Magnetic, cloud

1. INTRODUCTION

In the past of astronomy CMEs are an extremely late boundary which is utilized from year 1970. In late examination, by numerous analysts saw that the sun oriented cycle 24 is most fragile than cycles 22 and 23. The sunlight based cycle 24 could created extraordinary geomagnetic storm and sun powered enthusiastic molecule (SEP) occasions are related with sun oriented peculiarity. Earth coordinated CMEs are the primary component of producing major geomagnetic storm. Space climate forecasts of different organizations are given the aggravation appearance on the Earth. The Earth coordinated CMEs that containing toward the south attractive



field part is skilled to begin geomagnetic storms. Gosling et al. (1990) concentrated on the reason's geomagnetic storms have produced that by generally brought about by CMEs peculiarities. Subsequently, best device of CMEs and shock appearance time at the Earth is wanted for expectation of room weather patterns. CME takes the time, appearance to the Earth about least in hour and most extreme in 1 to 6 days. Different engendering models of CMEs and shock are utilizing for space climate variety gauge. Gopalswamy et al. (2001) introduced a model that space speed of CMEs in interplanetary medium with sun oriented breeze diminishes around 1 galactic unit. A comparable CMEs engendering model that considers unequivocally the impact of the drag force by the sun oriented breeze on the CMEs has been recommended (Vrsnak and Gopalswamy, 2002; Borgazzi et al., 2009). Concentrates on utilizing different strategies to follow the CMEs proliferation have found proof on the side of the drag force model (Byrne et al., 2010; Mostl et al., 2014).

Owens and Cargill (2004); Colaninno et al. (2013) anticipated a model for appearance of tempest towards Earth around 12 hours. Gopalswamy et al. (2001) might be contrasted with given this model. Hess and Zhang (2015) introduced a drag model that is capable gave the appearance of CME ejecta around 1.4 to 3.3 hours at Earth. Geomagnetic tempests can be classified, as far as geomagnetic movement file (Dst), into three classifications: (1) significant (extraordinary or extraordinary) storms, least Dst (Dstmin) of -100 nT or less; (2) moderate tempests, Dstmin falls somewhere in the range of -50 and -100 nT; and (3) frail tempests, -30 nT < Dstmin storm (Dstmin < -73 nT) related with a coronal mass launch (CME) and a determined shock in sunlight based cycle 24 happened on 6 April 2010, which was related with a CME occasion on 3 April 2010 (e.g., Möstl et al. 2010; Liu et al. 2011; Wood et al. 2011).

The main major geomagnetic storm in sun powered cycle 24 happened during 05-06 August 2011 (Dstmin = -107 nT), and the second and third major geomagnetic storms happened during 26-27 September 2011 [Dstmin = -101 nT (e.g., Wu et al. 2016a)] and 24-25 October 2011 (Dstmin = -132 nT), separately (e.g., Wood et al. 2016). There were five significant geomagnetic storms kept in 2012 alone, however just two significant geomagnetic storms were kept in 2013: one (Dstmin = -132 nT) on 17 Walk 2013 (Wu et al. 2016b) and the other one on 1 June (Dstmin = -119 nT). In the beginning stage of sun based cycle 24, the most serious tempest happened during 07-08 Walk 2012. This tempest's Dstmin reached -143 nT. The principal super geomagnetic tempest of sunlight based cycle 24 didn't happen until the declining stage on 17 Walk 2015 (e.g., Gopalswamy et al. 2015; Kamide and Kusano 2015; Individualized structure oka et al. 2015; Liu et al. 2015; Ramsingh et al. 2015). It is notable that the toward the south part of the interplanetary attractive field (IMF) assumes a significant part in the age of geomagnetic storms (e.g., Tsurutani et al. 1988; Tsurutani 1997). An enormous toward the south IMF can be related with various types of sun powered breeze structures: (1) an interplanetary (IP) shock wave (sheath) (e.g., Tsurutani et al. 1988; Kamide et al. 1998; Wu and Lep-ping 2008, 2016), (2) an attractive cloud (MC) (e.g., Wu and Lepping 2002a, b) or an IP coronal mass launch (ICME) (e.g., Richardson and Stick 2011; Wu and Lepping 2011), a heliospheric current sheet area limit crossing (e.g., McAllister and Crooker 1997), or (4) a blend of these interplanetary designs (e.g., Tsurutani and Gonzalez 1997; Echer and Gonzalez 2004). Among these, MCs are the most geoeffective in light of the fact that they by and large contain an enormous, durable toward the south IMF (e.g., Wu and Lepping 2008, 2016). Around 90 % of MC occasions are asso-ciated with geomagnetic storms. A MC occasion incorporates the actual



MC, typically an upstream shock wave with a sheath (district between the shock and the MC) (e.g., Wu and Lepping 2002a, 2011; Wu et al. 2015). Most sun powered cycle 24 major tempests (88 of them) are related with an ICME or a MC (Zhang et al. 2007; Wu et al. 2013). A geomagnetic tempest can be incited by (1) the MC sheath, (2) the main (i.e., forward portion) locale of a MC, (3) the following piece of a MC, and (4) both sheath and MC districts (e.g., Wu and Lepping 2002a). It is viewed that as the least worth of the z part of the IMF (B_{zmin}) inside a MC is very much related with the power of a geo-attractive tempest (Dst_{min}) (e.g., Wu and Lepping 2002a, 2002b, 2015, 2016); we think about the zGSE-part. Consequently, estimations of B_{zmin} in the sun oriented breeze can be utilized to foresee Dst_{min} (e.g., Wu and Lepping 2016). According to W. Gonzalez et al. (1994; B. T. Tsurutani & Gonzalez, 1997), geomagnetic storms are dangerous disturbances brought on by the effects of solar wind structures on the Earth's magnetic field and ionosphere. These disruptions are capable of impairing the functionality of both space- and ground-based technological systems under extreme geomagnetic conditions (Echer et al., 2005; NRC; Poppe & Jorden, 2006). Therefore, in order to design future capabilities for maintaining technological systems under extreme geomagnetic conditions, it is necessary to have an understanding of the underlying physical processes of the interplanetary drivers of geomagnetic storms. Coronal mass ejections (CMEs) and high-velocity plasma streams from solar coronal holes are the two solar features that cause geomagnetic storms (Gopalswamy). B. T. Tsurutani et al., 2011; et al., 2009). Interplanetary CMEs (ICMEs) are the interplanetary remnants of CMEs that travel from the solar coronal surface to the Earth via the interplanetary medium (Gopalswamy et al., 2001; Illing & Hundhausen, 1986). Thus, the term "ICME" will be used throughout the remainder of this study. Magnetic cloud and sheath fields, or the turbulent magnetic field areas that are frequently sandwiched between a shock and the leading edge of an ICME (Colburn & Sonett, 1966), are two subsets of an ICME (Burlaga et al., 1981; Lepping et al., 1997, 1991, 2015). A shock wave forms in front of an ICME when it moves sufficiently faster than the solar wind plasma that came before it. A shock is recognised by sudden changes in solar wind plasma properties and the interplanetary magnetic field (IMF). Co-rotating interaction regions (CIRs), on the other hand, are generators of fast streams from the coronal holes. A high-pressure area is created when the plasma is compressed by the fast stream's leading edge.

Total electron content (TEC) and electron density are two ionospheric metrics that can be considerably changed by a geomagnetic storm's effects on the ionosphere. The number of integrated electrons along a TEC unit cross-sectional region segment between the Worldwide Route Satellite Framework (GNSS) satellite and the beneficiary (Hofmann-Wellenhof et al., 1994); 1 Detective Unit (TECU) is 10¹⁶ electrons/m². 1 TECU variety can cause range blunders in the request for 0.163 m to GNSS signals at L1 channel (1.5754 GHz) (Galav et al., 2010; Klobuchar, 1996). Moreover, fast exhaustions of Sleuth are the proof of the events of ionospheric inconsistencies (Valladares et al., 1996). These anomalies in all actuality do cause shines of radio waves (Wernik et al., 2003). Shine impacts on trans-ionospheric radio transmissions can prompt transmission mistakes or through and through signal misfortune (A. O. Akala et al., 2012; Horvath and Crozier, 2007). At daytime in the tropical area, the qui-et-time zonal electric field is toward the east coordinated and toward the west coordinated around evening time. The upward inspire of $E \times B$ float for a toward the east coordinated electric field at the attractive equator and the resulting dissemination of plasma along the attractive field lines because of strain inclination and gravity powers cause the development of two pinnacles of plasma thickness (peaks) during



the activity of the forward wellspring at about $\pm 15^\circ$ of the attractive equator and a decreased plasma thickness at the attractive equator (box) (Appleton, 1946). This is the central ionization peculiarity (EIA) peculiarity, displayed by Balan and Bailey (1995) and Balan et al. (2009) by their Sheffield College Plasmasphere-Ionosphere Model (SUPIM). Nonetheless, around evening time, the zonal electric fields become toward the west coordinated, causing a descending direction of the ExB float prompting an opposite plasma wellspring activity. The opposite plasma wellspring was first displayed by Balan and Bailey (1995) and Balan et al. (2009), utilizing their SUPIM model, and approved by different creators, for example, Oyedokun et al. (2020). At the point when the converse plasma wellspring is areas of strength for adequately, related in reverse plasma flow separates the double pinnacle design of the EIA and mixes it into a solitary top around the attractive equator. Then again, when it isn't sufficient, the equator-ward transport of plasma ionization may not get to the attractive equator yet becomes recombined en route at latitudinal areas close to the magnetic equator in the two halves of the globe to shape minor central peaks (Balan and Bailey, 1995; Balan et al., 1997; Hanson and Moffett, 1966). In contrast to the African area, the reactions of the American and Asian tropical/low-scope ionosphere to geomagnetic storms have been all around considered (e.g., Essex et al., 2002; Fagundes et al., 2016; Xu et al., 2007). Ionospheric reaction to geomagnetic storm is positive when the upsides of ionospheric boundaries during geomagnetic storm offset the ostensible qualities during calm periods, and negative when going against the norm (Fagundes et al., 2016; Matamba and Habarulema, 2018). De Abreu et al. (2010) contemplated ionospheric reaction in the Brazilian area to the geomagnetic tempest of the April 5-8, 2000 and ascribed the period of Sleuth reaction to geomagnetic tempest to provoke entrance electric field (PPEF) direction. During geomagnetic storms, motional sun oriented breeze electric field infiltrates instantly into the magnetosphere, and becomes conveyed to the ionospheric polar district, from where it streams to the mid-scope locale, and afterward to the low-scope and tropical areas (B. T. Tsurutani et al., 2008). Therefore, this tempest time electric field is alluded to as PPEF. PPEF is significantly bigger than the ordinary ionospheric electric field that is related with the peaceful time wellspring impact (B. T. Tsurutani et al., 2008). The direction of PPEF, which relies upon the direction of IMF Bz, characterizes the period of an ionospheric reaction to a geomagnetic storm. At the tropical/low-scope district, at nearby daytime during geomagnetic storms, when IMF turns toward the south, PPEF is toward the east coordinated, and toward the west coordinated around evening time. The toward the east direction of PPEF escalates ionospheric forward plasma wellspring (Fagundes et al., 2016; Huang et al., 2005; Kikuchi et al., 2008), while the toward the west direction of PPEF drives a converse wellspring (A. O. Akala et al., 2020), causing decrease in ionospheric plasma thickness around the EIA peak and ensuing equator-ward development of the EIA peaks (Narayanan et al., 2013). Beforehand, in the African area, Adewale et al. (2011) concentrated on the reactions of African low-scope ionosphere to geomagnetic storms during 2000-2007 at Libreville, Gabon. The creators revealed blended reactions of positive and negative stages to the geomagnetic storms investigated. Likewise, A. O. Akala et al. (2013) explored the reactions of African central/low-scope ionosphere to the extraordinary geomagnetic storms that happened during the rising stage (2011-2012) of sun oriented cycle 24. The creators inferred that every one of the tempests were related with CME fields. Detective qualities were likewise answered to display positive reactions to the tempests. Every one of the past investigations on the reactions of the ionosphere to geomagnetic storms at the African



central/low-scope district primarily viewed as not many geomagnetic tempests and restricted stations. To this end, the ongoing work is quite extended in scope. Besides, the advanced best in class worldwide ionospheric Sleuth planning capacities (e. g. openmadriral.org) are accessible for iono-spheric examinations. Be that as it may, in these worldwide ionospheric Detective planning systems, Africa is profoundly under-rep-disdained because of lacking organizations of ionospheric sensors in the mainland, and these observational holes On the global TEC maps, they stand out quite a bit. This makes it still acceptable to use standalone GNSS receivers for ionospheric observations in Africa. This paper's major goal is to examine the interplanetary causes of a few specific, powerful geomagnetic storms that occurred during solar cycle 24 and the ionosphere's reactions in Africa, which is equatorial and low-latitude.

Table 1
Geomagnetic Storms Classification

Storm classification	Threshold
Very intense	SYM-H \square -200 nT
Intense	-200 nT \square SYM-H \square -100 nT
Moderate	-100 nT \square SYM-H \square -50 nT
Weak	-50 nT \square SYM-H \square -30 nT

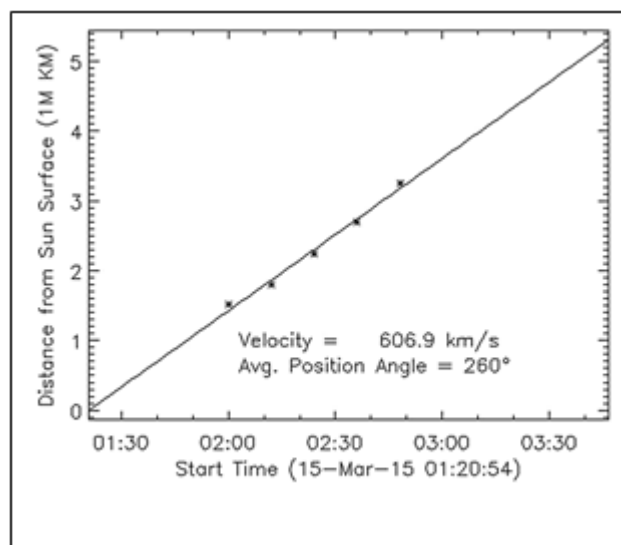
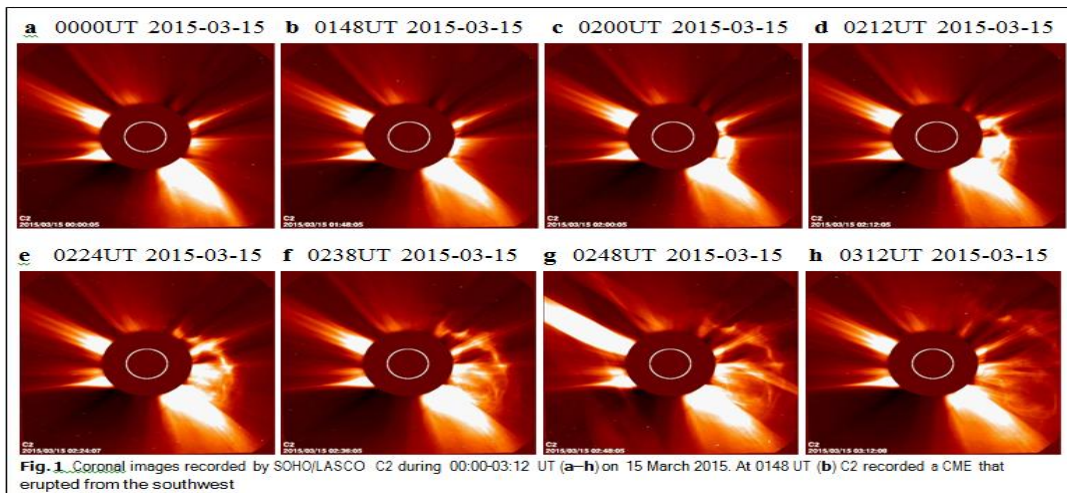
Observations

Propagation of CMEs near the Sun

Figure 1 shows a grouping of white-light coronal pictures recorded by SOHO/LASCO C2 during 00:00-03:12 UT on 15 Walk 2015. C2 recorded a CME (named CME15, henceforth) that emitted from the southwest at 01:48 UT (Fig. 1b) and showed up as a fractional radiance CME during 02:12-03:12 UT (Fig. 1d-h) in the field of view (FOV) of C2. CME15 was related with a C9.1/1F flare (S22W25) and a progression of type II/IV radio explodes. The underlying engendering pace of CME15 was ~606 km/s (see Fig. 2). SOHO/LASCO C3 recorded the CME15 at 02:18 UT (Fig. 3a) in the FOV. Figure 3a-c shows the advancement of CME15 during 02:18 UT-06:06 UT on 15 Walk 2015. The typical speed of CME15 in the C3 FOV was 668 km/s. shows the in-situ sun based breeze plasma, attractive field (estimated by the Breeze shuttle), and the Dst file during 16-18 Walk 2015. The Breeze space apparatus recorded an interplanetary (IP) shock (we will allude to this shock as Shock17, set apart by a strong vertical line in Fig. 4) at 03:57 UT on 17 Walk 2015, and a transition rope up-and-comer a couple of hours after the intersection of Shock17. Utilizing a MC-fitting model (Lepping et al. 1990), Table 1 records the best-fit results for the MC (we will allude to this MC as MC17). Figure 5a, b shows MC17's attractive field structure in cloud arranges and GSE organizes, separately. The strong dark bends are the MC-fitting outcomes. MC17 began at 10:36 UT (set apart by an upward ran line with a sharp change in B_y and ϕ_B) and finished at 23:36 UT (set apart by an upward strong line where there is a sharp drop in $|B|$) on 17 Walk. The limits of a MC are generally demonstrated by sharp changes in field point (θ_B or ϕ_B) or in field extent, $|B|$. The span (Δt_{MC}) of MC17 is

13.00 h, which is ~30 % more modest than a typical MC at 1 AU, $\Delta t_{MC} = 18.82$ h, (e.g., Lepping et al. 2015; Wu and Lepping 2015). The length of the sheath is around 7 h. The MC17 fitting outcomes are showed

Fig 1



both in Table 1 and Fig.2 As we can see, the directional portion of the fit is between reasonable and good, especially in cloud (CL) coordinates, while the B-magnitude portion of the fit is subpar: The observation has a double peak, whereas the model does not. The profile of B is shown in the bottom panel of Fig. 5a, and as needed by cloud coordinates, B is nearly flat (second panel from bottom). This indicates that the model-field centre of the MC17 was in the actual centre. However, because the MC's magnetic field noise level, R (Lepping et al. 2003), was high ($R = 0.244$), we categorise MC17 as a quality 3 MC in accordance with the concept of MC quality (Q_0) (Lepping et al. 2006). When an MC's R is larger than 0.215, the MC will have a quality of 3. At 04:45 UT, the sudden storm commencement (SSC) caused by Shock17 began. The moment the IMF turned southward, the value of Dst began to fall. During the passage of the sheath (the area between the IP shock and the driver of the IP shock), the storm grew stronger (Dst dropped to 80 nT at 10:00 UT). Shortly after the IMF

shifted to the north, the storm later had a minor recovery (i.e., Dst decreased to 50 nT). The magnetic cloud (MC)'s substantially negative Bz forced the IMF to move southward once more a few hours later, which caused the second storm to intensify and reach Dst = 223 nT on March 17. We determine that the A two-step storm will occur on March 17 for St. Patrick's Day. The second step was connected to a southern MC field, whereas the first step was connected to a southbound IMF embedded in the sheath area.

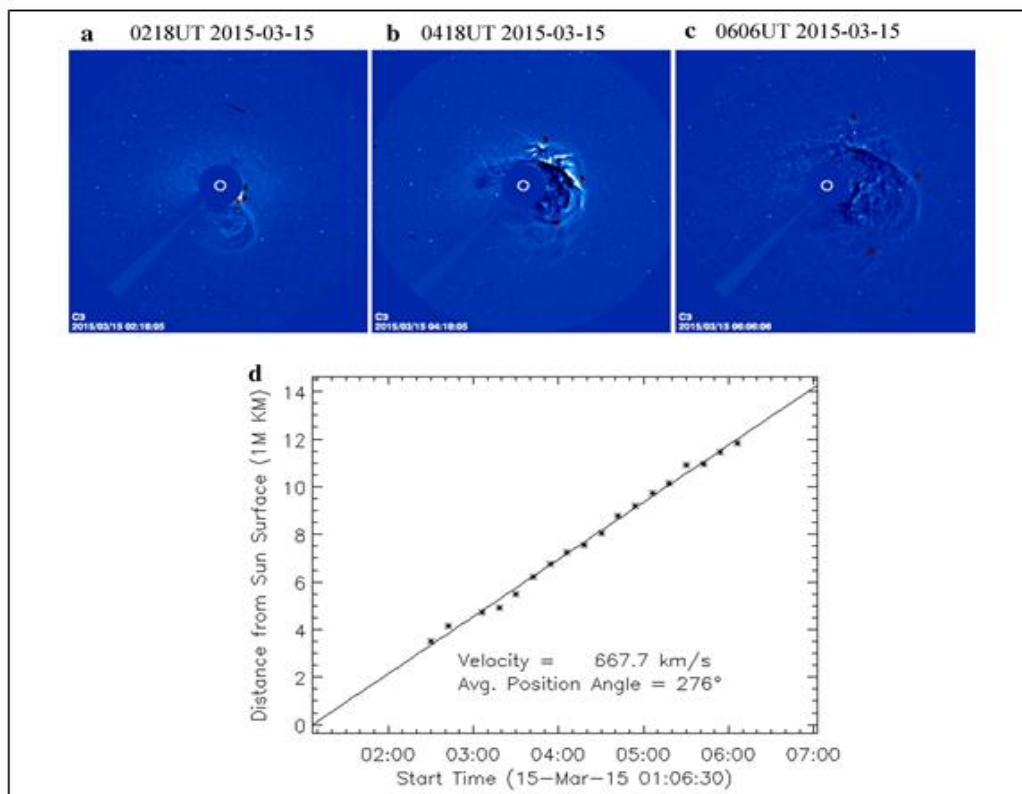


Figure 3

Propagation/evolution of the CME and its driven shock

From 606 km/s in the C2 FOV (2.5-6.0 Solar radii, Rs), to 668 km/s in the C3 FOV (3.7-32 Rs), to 706 km/s between 18.82 and 211 Rs ($V_{18.82-211Rs} = 706$ km/s, at 06:06 UT on March 15, CME15's leading edge was at 18.82 Rs (Fig. 3d, page). It should be noted that the CME propagation speed determined by C2 or C3 was the anticipated speed on the sky's horizontal plane. Although the expected speed has been adjusted for the direction of the CME, mistakes could still remain and add to the uncertainty of the estimated arrival time. The location of the CME and the speed at which its driven shock is spreading are shown in Table 2. Keep in mind that the measurements made by Those above the solar surface are C2 and C3. These findings imply that the CME's propagation speed was comparable in the areas of 18.8-211 Rs and 6.95-18.8 Rs.

In the vicinity of 6.95-211 Rs, respectively, the calculated propagation speeds of Shock17 and the ICME17 were 797 and 702 km/s. Upstream and downstream of the IP shock, the in situ solar wind speed was 400 and 500 km/s, respectively. The sheath's speed ranged from 500 to 600 km/s, while the plasma's average speed across the MC was 550 km/s. Based on C3 observations, the predicted ICME propagation period to the Earth was 58.96 h, or " $204.05 \frac{6.95}{105} \frac{105}{(668 \cdot 3600)} = 58.96$ h." Consequently, the ICME would arrive at the Earth on March 17, 2015, at around 15:09. According to the Wind measurements, the CME propagated from the



Sun to 1 AU in just 56.13 hours. incorrect propagation time data

2. Data and Methods

We chose and examined eight serious geomagnetic storms that happened during sun powered cycle 24. For each tempest, to look at the sun oriented breeze plasma highlights during various tempest's stages (beginning, principal, and recuperation stages), our informational indexes cover 11 days: 5 days before the day of the tempest's fundamental stage, day of the tempest's primary stage, and 5 days later. Likewise, the geoeffectiveness of each tempest was explored by reviewing the degree of tempest stage influ-ences of each tempest on the ionosphere over the review locales. The ICMEs considered were the interplanetary leftovers of the Radiance CMEs (Gopalswamy et al., 2007; Yermolaev and Yermolaev, 2006). They for the most part have directional effect and exceptionally geoeffective on the Earth (Gopalswamy, 2006; Gopalswamy et al., 2007; Gopalswamy, Yashiro et al., 2015). The ICMEs information were acquired from The high goal 1-min arrived at the midpoint of IMF B (nT), IMF Bz (nT), and sun oriented breeze plasma information; speed, Versus((kms⁻¹), thickness, DS (n/cc), temperature, TS (K), stream pressure, PS (nPa), electric field, Ey (mV/m), and SYM-H file (nT) were gotten from. The Kp list information were gotten from We analyzed interplanetary circumstances for each geomagnetic storm utilizing the measures underneath. The ICME drifters' cases were distinguished by two head geoeffective parts; attractive cloud and sheath fields (Myllys et al., 2016). Sheaths are fields behind a shock wave. At the point when IMF turns toward the south simultane-ously with sharp expansions in normal greatness of IMF (IMF B) and all sun oriented breeze plasma boundaries, a forward shock is framed and when there is a diminishing in all IMF and sun powered breeze plasma boundaries, aside from an expansion in Versus, an opposite shock is shaped (Echer and Gonzalez, 2004; W. Gonzalez et al., 1994). The two sorts of shocks are related with sheath fields. Attractive mists are portrayed by low TS and DS, high mag-netic field strength with smooth turn of IMF at 180° (south to north or east to west) (Manchester IV et al., 2017), went before by shocks and sheath fields (Burlaga et al., 1981; Lepping et al., 1990). Further, CIRs are indications of high velocity streams from coronal openings floating over more slow stream of plasma. CIRs are analyzed by the toward the south direction of IMF (Bz < 0), sharp expansions in normal IMF B and sun oriented breeze plasma boundaries, with the exception of Versus and TS, which are postponed prior to picking up speed and increment sometime in the future unique in relation to when normal IMF B and other sun powered breeze plasma boundaries expanded (J. T. Gosling and Pizzo, 1999; Hutchinson et al., 2011).

Switzerland (Ciraolo et al., 2007). The extricated incline Detective information were con-verted to vertical Sleuth utilizing the planning capability with the supposition that the ionospheric puncture point level is at 350 km (Mannucci et al., 2005). Figure 1 shows the African central/low-scope stations utilized for this review. The GNSS recipients' geographic and attractive organizes; and stations' time regions are recorded in Table 2. To decide the degree of Sleuth reactions to the periods of the geomagnetic storms at each station, we looked at the mean of the peaceful days (Kp □ 3) Detective infomation throughout the long stretch of event of each geomagnetic storm with Detective qualities for each period of each geomagnetic storm (A. O. Akala et al., 2013; Hajra et al., 2016).

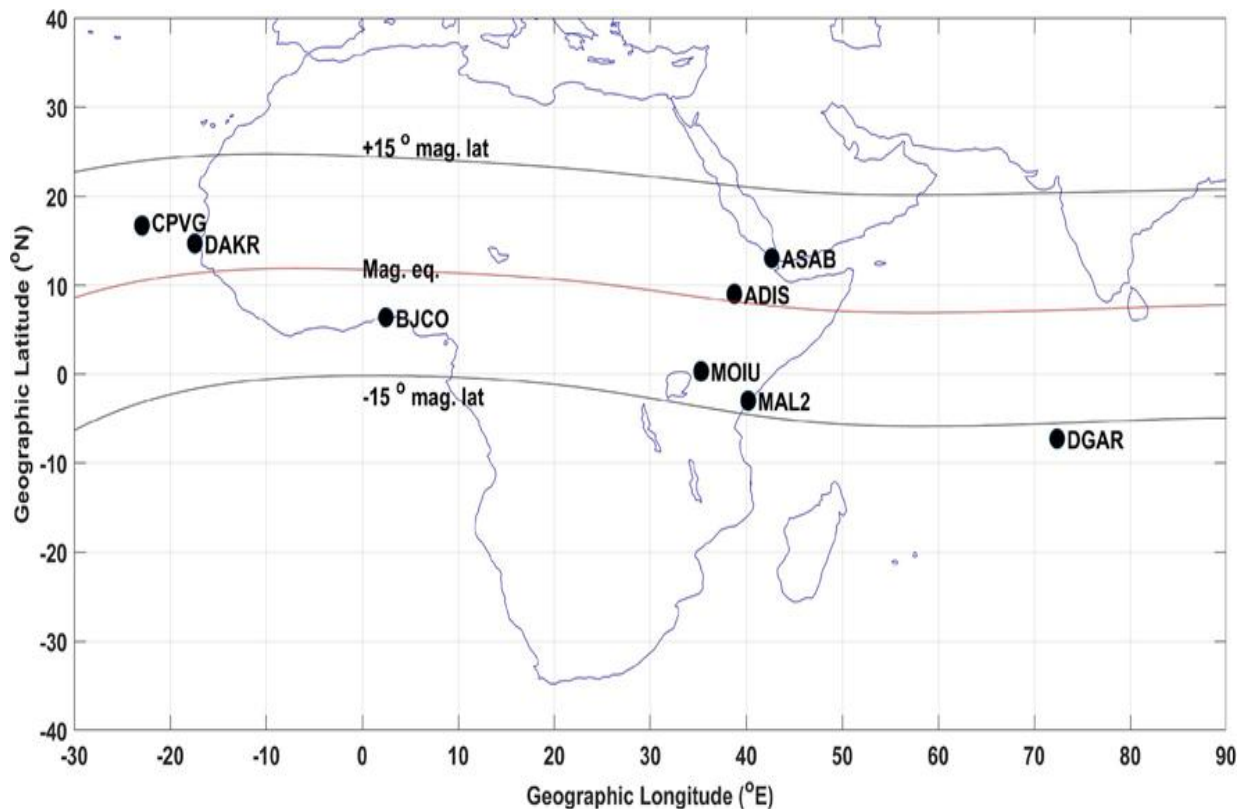
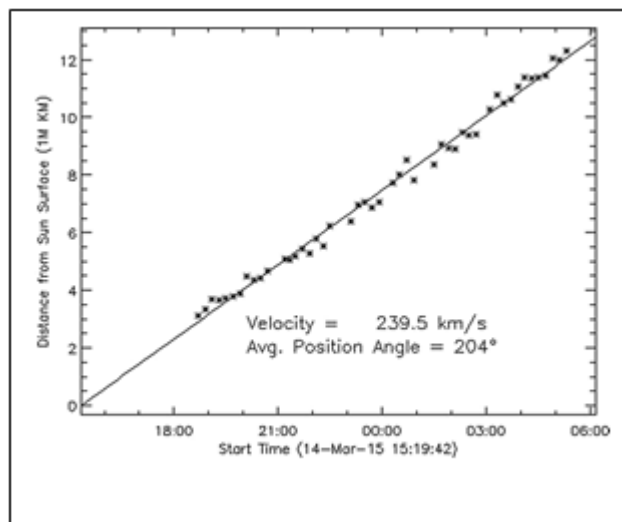
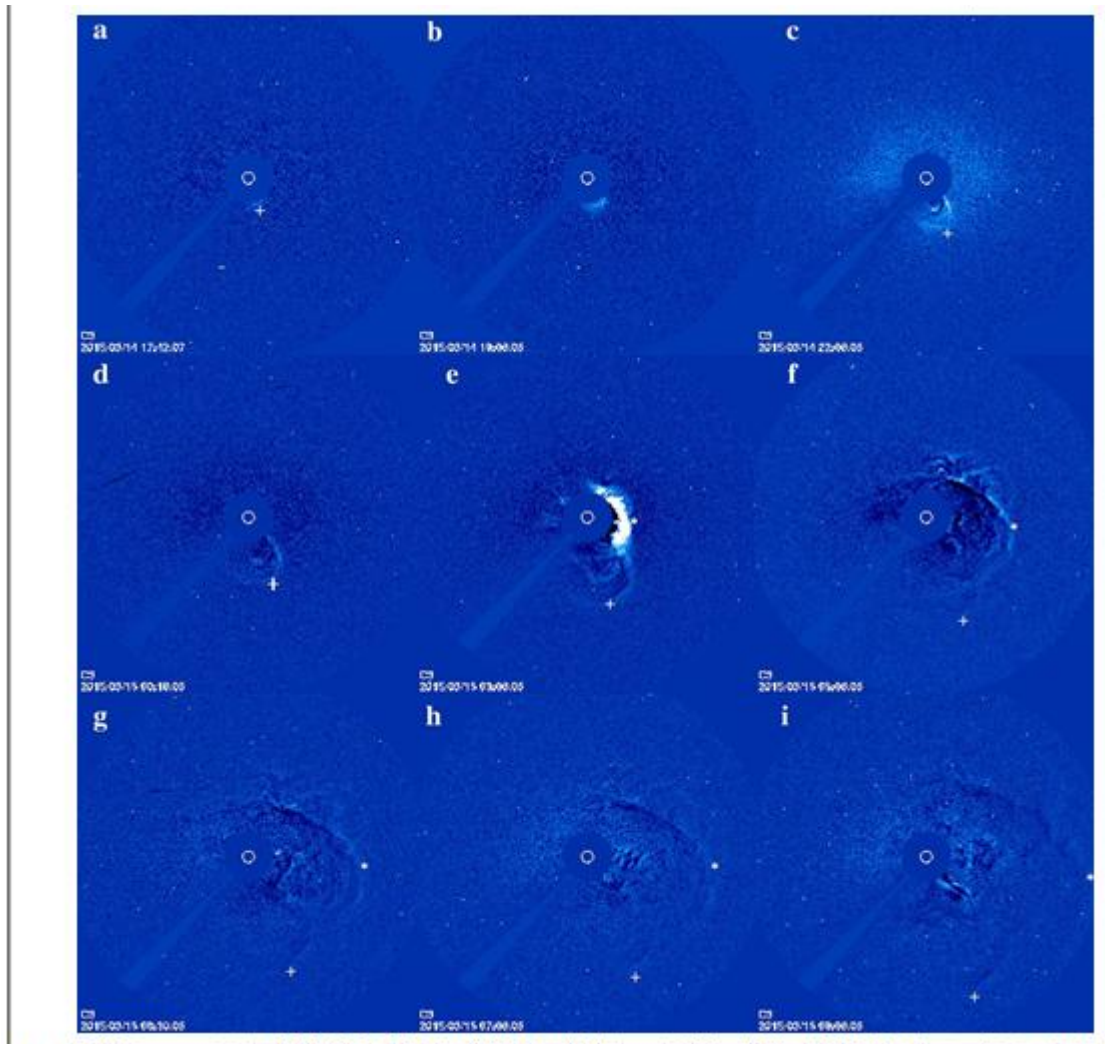


Figure 4. Map Showing the GPS Stations: CPVG (Cape Verde), ASAB (Asab), DAKR (Dakar), ADIS (Addis Ababa), BJCO (Cotonou), MOIU (Eldoret), MAL2 (Malindi) and DGAR (Diego Garcia). The red line indicates the magnetic equator. GPS, global positioning system.

Moreover, GNSS glimmer information from two stations: Addis Ababa and Dakar for a really long time 2011 and 2013 were gotten by Novatel GSV4004 B GNSS collectors, worked at a 50 Hz inspecting rate. The recipients at the same time followed Worldwide Situating Framework (GPS)

Solar source of the super- storm on 17 March 2015

For certain scientific societies [such as the International Study of Earth-affecting Solar Transients (ISEST) for Variability of the Sun and Its Terrestrial Impact (VarSITI)], the solar source of the superstorm of March 17, 2015, is a hot issue. In attempt to find the solution, earlier CME photos were examined, and on March 14, 2015, a sluggish CME—designated CME14—was discovered. CME14 was initially discovered by SOHO/LASCO C3 at 17:43 UT. Figure 7 displays a series of CME photos captured by SOHO/LASCO C3 between 17:42 and 09:06 UT on March 14, 2015. The letters "+" and "" denote, respectively, the leading edges of CMEs 14 and 15 (this CME erupted on March 15, 2015). The CME14's speed was 240 km/s or slower (see Fig. 8). Figure 7e demonstrates that C3 saw CME15 on the right (or west) and CME14 on the bottom (or south), respectively. After 07:30 UT on March 15th, the leading edge of CME15 crossed the leading edge of CME14 (see Fig. 5g-j).



Since CME14 and CME15 propagated outside of the C3 FOV, no CME image was available to confirm it.



Additionally, CME14's direction of propagation (towards the south/bottom) and CME15's direction of propagation (towards the west/right) were different. Finally, Fig. 7f-i clearly demonstrates that CME14 was propagating in its own direction (southward projected on the plane of sky) after the leading edge of CME15 passed the In addition to the aforementioned three factors, CME14's speed (240 km/s) prevented it from striking Earth before March 18, 2015. CME14 would proliferate from 7 Rs in at least 7 days.given that the speed was 240 km/s, to the Earth. This indicates that CME14 would miss Earth by March 21, 2015. For these grounds, we came to the conclusion that the CME15-driven southward field in the sheath and a portion of MC17 was what created the superstorm on March 17, 2015.

3. DATA COLLECTION SOURCES

We picked areas of strength for eight tempests that happened in daylight based cycle 24 and dissected them. Our educational assortments for every whirlwind length 11 days: 5 days before the day of the storm's huge stage, the day of the storm's central stage, and 5 days after to explore the sun arranged breeze plasma features during different whirlwind's stages (starting, essential, and recovery stages). Additionally, how much every's storm stage impacts on the ionosphere over the survey regions was dissected to choose the geoeffectiveness of every whirlwind. The interplanetary extras of the Brilliance CMEs were the ICMEs that were contemplated (Gopalswamy et al., 2007; Yermolaev and Yermolaev, 2006). They normally impact the Earth in a planned manner and are very geoeffective (Gopalswamy, 2006; Gopalswamy et al., 2007; Go-Yashiro Palswamy and accomplices, 2015). The significant standard 1-min showed up at the midpoint of IMF B (nT), IMF Bz (nT), and sun situated breeze plasma data were used to make the ICME data; the speed, thickness, DS (n/cc), temperature, TS (K), stream pressure, PS (nPa), electric field, Ey (mV/m), and SYM-H list (nT) were used to make various variables. This paper taken hourly information of charming field (B), sun organized breeze speed (v), Aggravation storm time (Dst) information from OMNI web of NASA correspondingly information of Grandiose shafts force (in hours) from Moscow ground based neutron screen having killed unbending nature ($R_c = 2.42\text{Gev}$) and locale on the Earth is expansion 55.47N, longitude 37.32E during the period from 10 Walk around 31 Walk around year 2015 in days. For CMEs information we have utilized CME catlog of NASA. Huge surge of appealing field and plasma from the Sun to interplanetary space could make storm. How different MCs were associated with the super- storm of 17 Walk 2015? We just perceived MC17 as the driver for the IP Shock17 of 17 Walk 2015. The MC17 was perceived in two extraordinary for cedars: (1) We at first applied the redid MC auto-obvious check (MCI) model (Lapping et al. 2005) to track down the MC competitor, and sometime later (2) we utilized a MC-fitting (MCF) model (Lapping et al. 1990) to pick as far as possible. interplanetary charming field, sun controlled breeze plasma, Residue report, and two or three instigated limits during 17-18 Walk 2015. The MCI model apparent a MC competitor, which is discrete by a level dull bar, and the MCF model had the decision to perceive a MC (MC17), which is limited between two vertical red lines, as displayed in Fig. 6d. The back uttermost spans of the MC17, as settled apparently, is predictable not for all time laid out by the MCI model, yet the MC17 front limit, as settled clearly, is around 4 h in front actually balancing out there by the MCI model. The shock driven by the MC17 (Shock17) is independent by an upward line Wind recorded ~24 h of low plasma beta (β) sun based breeze material between ~12:00 UT on Walk 17 and ~12:00 UT on Walk



18. The low β region was sepa-evaluated by an appealing opening, which happened near the fruition of 17 Walk (showed by spotted and ran lines). Notwithstanding the MC17's entirely honest intentions limit, there was a ~ 12 -h low β stretch (set to the side in orange tone and "ICME ?" in Fig. 6b). Utilizing the MCF model, we can't get serious areas of strength for a for this district considering the way that the engaging field didn't sway a lot of in heading (i.e., θ_B or ϕ_B didn't change a ton) inside this region (see Fig. 6e, f). Other than the lack of sig-nificant field turn there, B_z was simply around zero in that period. Similarly, we mulled over that the super-storm on 17 Walk 2015 was accomplished by the toward the south field in both the sheath and the MC17. The results of this study are trustworthy with the new work by Karaoke et al. (2015), however are not identical to the outcomes wrapped up by Gopalswamy et al. (2015),

4. RESULT AND DISCUSSION

The CMEs is one of the really transient highlights of the Sun. CMEs simply changes into ICMEs when bury in heliospheric space. The figure 1 shows the pictures of sun based yield variety from 10 Walk to 15 Walk 2015. On 15 Walk 2015 these Earth-coordinated CMEs blasts bury into interplanetary space disturbed the space climate. Interplanetary attractive field (B) and interplanetary power field (VB) shows comparative action and great positive relationship during a similar timeframe which have displayed in figure 2 and 5. Interplanetary field lines change the track of charged particles in heliosphere. Table shows the SOHO/LASCO Radiance CMEs (Coronal mass discharges) their related sun oriented flare occasions during period from 10 Walk to 31 Walk of year 2015. Sun based flares have high energy particles and radiation that are perilous for human. The attractive field lines of Earth are safeguarded from the impacts of charged particles sun powered flares and other sun oriented movement which happened by the Sun too. The most perilous peculiarities of the Sun is X class flares storm which is extremely hazardous. The perilous x class flares stringently forestalled by field line of Earth. The flares storm made an unsettling influence at Earth encompassing that is ionosphere coming about obliterate media transmission. Alongside fiery bright radiation, they heat the World's external environment, making it grow. This caring unsettling influence switches the hauling of satellites up Earth. Likewise, both extraordinary radio discharge from flares and these progressions in the climate can corrupt the accuracy of worldwide situating framework (GPS) estimations. The modest number of exceptionally high energy particles that arrives at the surface doesn't altogether build the degree of radiation that individuals experience consistently. The most over the top upsetting occasion of this planet on human movement is known as geomagnetic storms are related with sun powered flares and plasma. Radiance CMEs now and then happened with and at some point are not. The interplanetary attractive field and interplanetary power assume a significant part in heliosphere have displayed in figure 2. The interplanetary attractive field and interplanetary power shows the similitude during time scale 10-31 Walk 2015. In this way it have great positive connection has displayed in figure 5. The extension of sunlight based discharge in sun oriented space could create sun powered breeze. The development sun oriented breeze around 450 Km/second in space from the Sun containing more charged particles that are electrons and protons and others particles. The Sun based breeze proliferation development right off the bat through the sun oriented coronal openings, which are dominantly happened close to the Sun's shaft. In figure 3 shows the progression of sun powered breeze speed during the period from 10-15 Walk 2015. The impact of sun



based breeze effect on our planet happened during dynamic district of Sun that is sunspot maxima at this stage sun powered breeze areas of strength for is may delivered storm comparing to flares and CMEs of the Sun. At the point when these corona CMEs and their related sun powered flares from 15-17 Walk 2015 arrived at close to the World's magnetosphere they tweaked the Cosmic enormous beams that approaching from interstellar medium. 4.

Date	CMEs Speed (Km/s)	CMEs associated solar flares
10 March 2015	1055	M 5.7
15 March 2015	725	C 9.4
24 March 2015	1800	None

IMF data, solar wind plasma data, SYM-H and Kp indices data, mean TEC data over the respective quiet days of the month of each geomagnetic storm's occurrence, TEC data for the 11 days leading up to the day(s) of the geomagnetic storm's occurrence, and TEC responses over the study locations to each of the eight intense geomagnetic storms are all displayed in Figures 2 to 9. In Figures 2 and 4, the scintillations' reactions to the storms were also depicted. On the diagrams, points A, B, C, and D stand in for storm sudden commencement (SSC), or the start of the storm's main phase, the conclusion of the storm's major phase, and the end of the storm's recovery phase, respectively. The traits are listed in Table 3. from among the eight geomagnetic storms. The crest station and the magnetic equator station, respectively, are represented by the station codes on the diagrams with the letters Cr. and Eq.

Table 2
GNSS Receivers' Geographic and Geomagnetic Coordinates and Stations' Time Zones

	Geog. lat (°N)	Geog. long (°E)	Mag. lat (°N)	Mag. long (°E)	Local time (h)	Station
Cape Verde	16.85	-25.02	6.02	96.55	LT = UT - 1	
Asab	13.01	42.70	4.86	114.39	LT = UT + 3	
Dakar	14.70	-17.44	3.08	89.16	LT = UT	
Addis Ababa	9.04	38.75	0.18	110.45	LT = UT + 3	
Cotonou	6.38	2.44	-3.08	74.53	LT = UT + 1	
Eldoret	0.52	35.28	-8.98	106.99	LT = UT + 3	
Malindi	-3.22	40.13	-12.67	111.79	LT = UT + 3	
Diego Garcia	-7.23	72.40	-16.84	142.88	LT = UT + 6	

GNSS, Global Navigation Satellite System

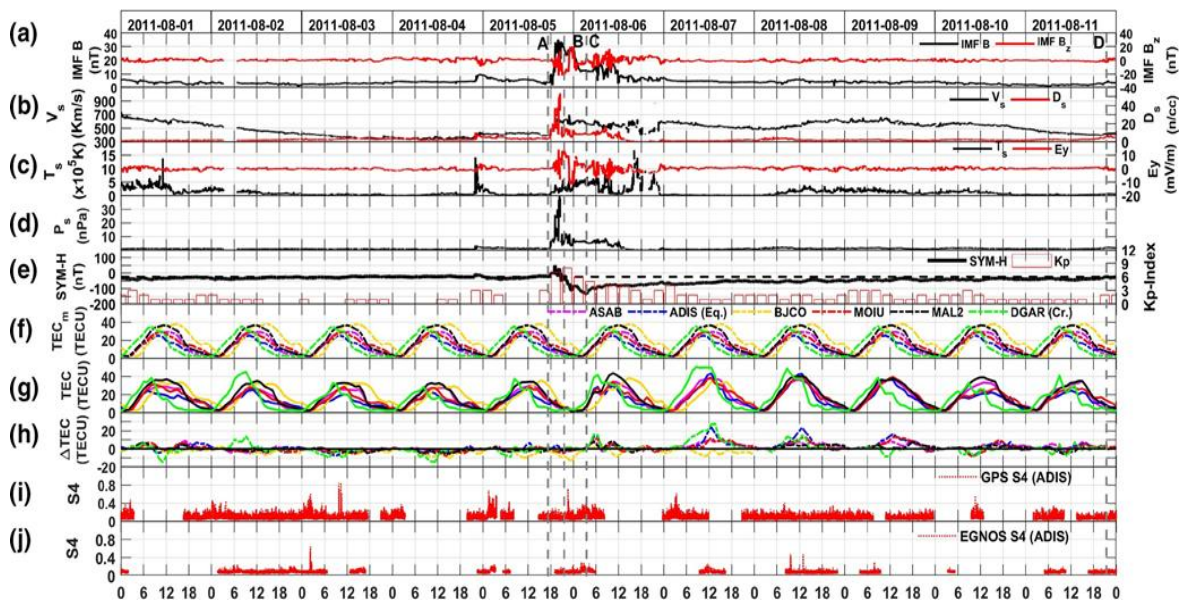


Figure 6 depicts the intense geomagnetic storm that occurred on August 6, 2011 (minimum SYM-H: 126 nT), with days from August 1 to August 11 on the x-axis for the following measurements: (a) average IMF B (nT) & IMF Bz (nT); (b) solar wind plasma speed, Versus (km/s) & solar wind proton density, Ds (n/cc); (c) solar wind plasma temperature, (f) changes in mean quiet days TEC (TECU) throughout the course of August 2011 for Asab, Addis Abeba, Cotonou, Eldoret, Malindi, and Diego Garcia, (h) deviations of mean quiet-time TEC from the storm-time TEC, (g) diurnal changes of TEC (TECU) throughout the 11 days linked with the storm, (i) Addis Ababa GPS S4 index Ababa and the Addis Ababa (j) EGNOS S4 index. On the diagram, the letters Cr. and Eq. stand for the crest station and the magnetic equator station, respectively. Storm sudden commencement (SSC) (the start of the storm's beginning phase), the start of the storm's main phase, the conclusion of the storm's main phase, and the end of the storm's recovery phase, respectively, are represented by the vertical dashed lines A, B, C, and D. TEC stands for total electron content; IMF is for interplanetary magnetic field.

Table 3 - List of halo - CMEs and Solar Flares Events during the period from 10 March to 24 March 2015.

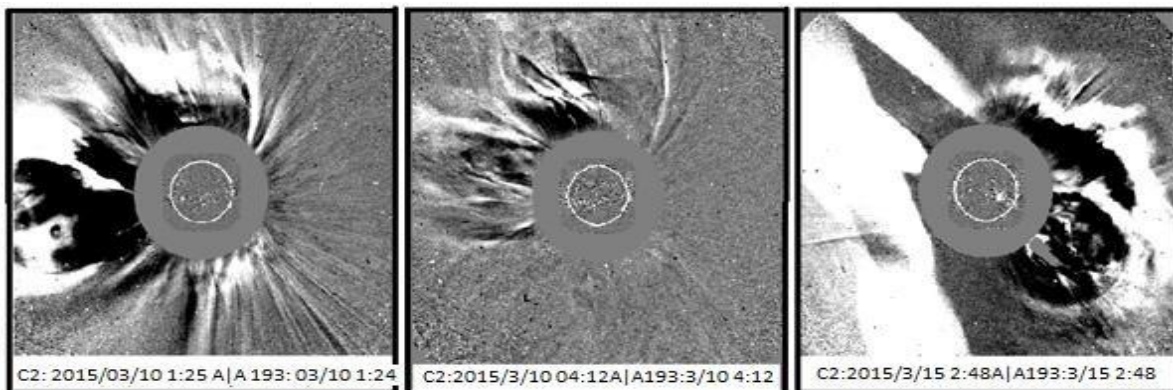
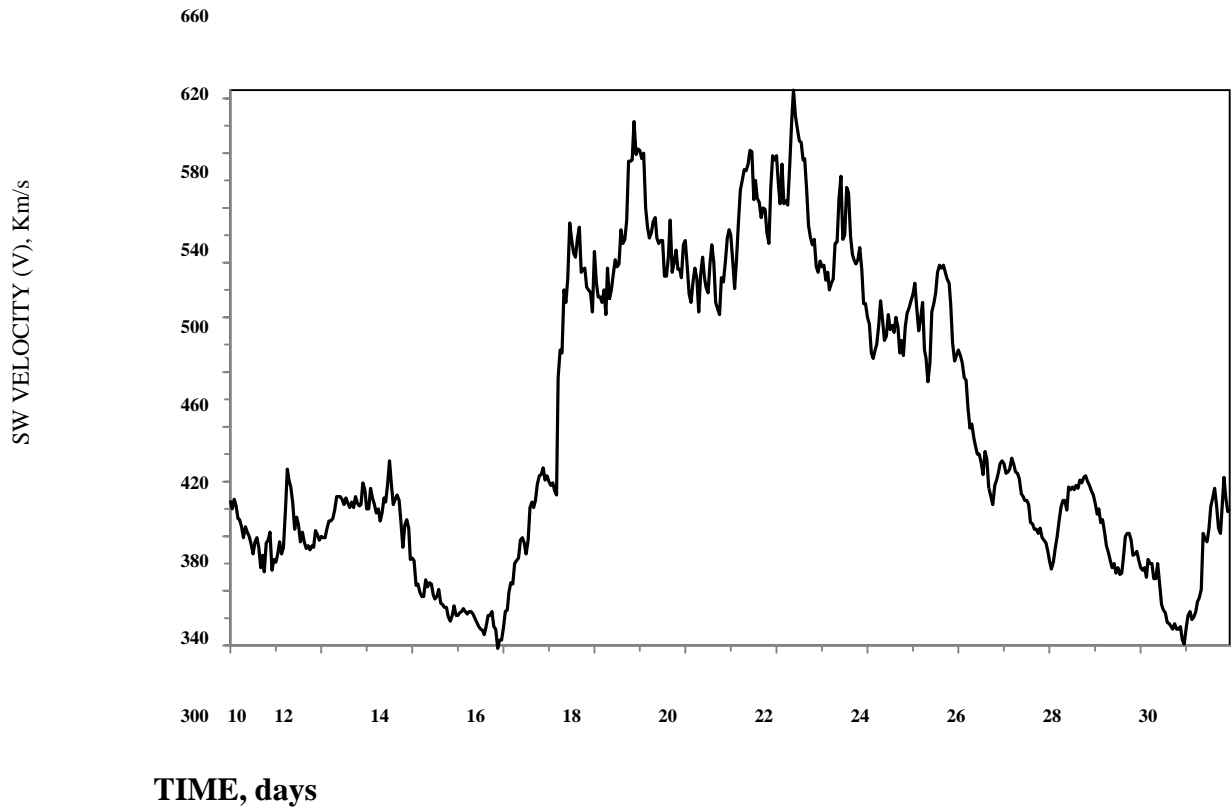


Figure 7: Time profile of IMF (B) and (VB) during the period from 10 March to 31 March 2015.



Figures 8: Time profile of Cosmic ray intensity (CRI) and Disturbance storm time (Dst) during the period from 10 March to 31 March 2015.

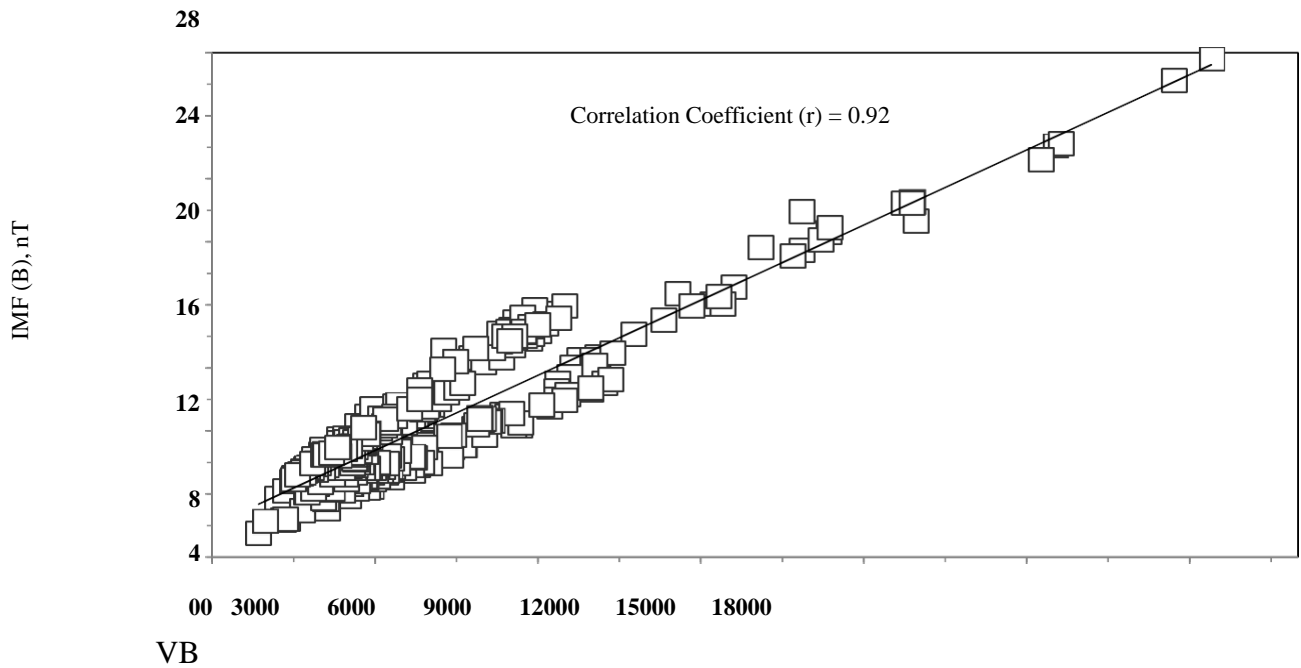


Figure 8: Cross plot between IMF (B) and VB during the period from 10 to 31 March 2015.



5. CONCLUSION

On Walk 17, 2015, corona CMEs and the sun oriented flares they produce arrive at the World's environment, causing geomagnetic storms, which are brief interruptions of the planet's attractive field. These tempests might upset our power frameworks, radio interchanges, GPS, and different frameworks. Hence, we ought to be worried that a serious CME on Walk 15 could set off areas of strength for a tempest on Walk 17, which could finish in overall calamity and put our lives in peril. The Sun's serious movement and the various startling and unexpected occasions that are happening on its surface demonstrate that we ought to be keeping watch for terrible. On "St. Patrick's Day" (17 Walk 2015), the first mega geomagnetic tempest of sun powered cycle 24 happened. The tempest's starting point can be distinguished as the sun oriented flare on Walk 15, 2015. On that day, at around 2:10 UT, SOHO/LASCO C3 saw an incomplete corona coronal mass discharge (CME) that was associated with a C9.1/1F flare (S22W25) and a line of type II/IV radio explodes. For the time period of 02:10-06:20 UT, the anticipated engendering rate of this CME is 668 km/s (see Fig. 1). At 03:59 UT on Walk 17, an interplanetary (IP) shock that was undoubtedly brought about by the related ICME arrived at the Breeze shuttle. The St. Patrick's Day occurrence was a two-step storm, we finish up. The sheath was associated with the initial step, though MC17 was associated with the second. CME15 was the sun oriented wellspring of MC17. Additionally, we found that utilizing the proper Dstmin assessment recipe On the grounds that sun based breeze speed, as well as Bs, has a critical impact in the figure of geomagnetic movement, it is fundamental for space climate expectations to have the option to gauge the power of MC-related geomagnetic storms. We explored the interplanetary beginning stages of eight serious geomagnetic storms during sun based cycle 24 and the responses of Criminal investigator at African focal/low-scope region to them, as well as the responses of tries to please of the whirlwinds at Addis Ababa and Dakar. Clearly, African tropical/low-scope Detective was changed by geomagnetic storms. The survey's essential choices are: 1. Six of the eight geomagnetic storms were driven by ICME strays: sheath fields, alluring fogs or both. Specifically, storms of 6th of August, 2011 and seventeenth of Walk, 2015 were driven by sheath fields, nineteenth of February, 2014 and thirteenth of October, 2016 whirlwinds were driven by appealing cloud fields, 10th of Walk, 2012 and first of January, 2016 whirlwinds were driven by a blend of sheath and appealing cloud fields. Two of the whirlwinds, first of June, 2013 and seventh of October, 2015 storms were driven by CIRs The responses of Investigator to the fundamental times of the whirlwinds were generally negative. All around, the time of African focal/low-scope Analyst response to geomagnetic storm is dependent upon the close by time of the geomagnetic whirlwind's spreading out and the storm's interplanetary driver. Despite geomagnetic whirlwind's power, the time of ionospheric response to geomagnetic storm is coordinated by the close by time of the geomagnetic storm's spreading out and the whirlwind's interplanetary driver. Also, with the several open flash data, the essential times of the geomagnetic whirlwinds of 6 August, 2011 and 1 June, 2013 didn't compel checked changes on shimmer occasions at Addis Ababa and Dakar, individual ly. It is imperative to make reference to that the starting hours of the central times of the two whirlwinds occurred during daytime (off PRE) hours, the period which is known not to be useful for L-band shimmer happen rences (A. O. Akala et al., 2012, 2017). Nonappearance of GNSS shimmer data in Africa is a critical cutoff for this survey. The future direction of using the Speed of progress of Investigator Rundown (ROTI) as mediator for ionospheric irregularities assessments is



recommended ICME-driven storms with daytime major stages caused the shaft ward transport of plasma from the mag-netic equator toward the EIA tops and the equator-ward improvement of plasma from the EIA daytime regions, for those with neighborhood evening essential stages. This is because daytime toward the east PPEFs cause forward wellspring increments, provoking enhancements of plasma thickness around the EIA pinnacles and reduction of plasma thickness around the appealing equator (Balan et al., 2009; Oyedokun et al., 2020). Conflicting with the standard, evening time toward the west PPEFs drives a contrary wellspring, causing decline in ionospheric plasma thickness around the EIA top and resulting equator-ward improvement of plasma (A. O. Akala et al., 2020; Fagundes et al., 2016) CIR-driven storms for the most part recorded negative ionospheric stages, no matter what the local time at which the whirlwind spread out. In addition, moderately, CIR-driven storms are less geoeffective than ICME vagrants driven storms. CIR-driven plasma is significantly more hot than ICME-driven plasma. A colder and denser plasma sheet recommends more grounded ring current in the Van Allen belt (Lavraud et al., 2006).

REFERENCES

1. Borgazzi A., Lara A., Echer E. and Alves M.V. "Dynamics of coronal mass ejections in the interplanetary medium", *Astro. and Astrophys.*, pp. 885-889, 2009.
2. Byrne J.P., Maloney S.A., McAteer T.J., Refojo J.M. and Gallagher
3. P.T. "Propagation of Earth- directed coronal mass ejections in three
4. dimensions", *Nature Communications*, 1, 74, 2010.
5. Colonnino R.C., Vourlidis A. and Wu, C.C. "Quantitative comparison of methods for predicting the arrival of coronal mass ejections at Earth based on multi view imaging", *J. Geophys. Res.*, pp. 6866-6879, 2013.
6. Gopalswamy N., Lara A., Lepping R.P., Kaiser M.L., Berdichevsky
7. D. and St. Cyr O.C. "Interplanetary acceleration of coronal mass ejections", *J. Geophys. Res., Lett.*, pp. 145-148, 2001. Gopalswamy N., Lara A., Yashiro S., Kaiser R.P. and Howard R.A., 2001. "Predicting the 1-AU arrival times of coronal mass ejections", *J. Geophys. Res.*, pp. 29207-29218, 2001.
8. Gosling J.T., Bame S.J., Mc Comas D.J. and Philips J.L. "Coronal mass ejections and geomagnetic storm", *Geophys. Res. Lett.*, pp. 901-904, 1990.
9. Hess P. and Zhang J. "Predicting CMEs ejecta and sheath front arrival at L1 with a Data-Constrained physical model", *J. Astrophys.*, pp. 144, 2015.
10. Mostl C., Amla K., Hall J.R., Liewer P.C., De Jong E.M., Colonnino R.C., Veronig A.M., Rollett T., Temmer M., Peinhart V., Davies J.A., Lugaz N., Liu Y.D., Farrugia C.J., Luhmann J.G., Vrsnak B., Harrison R.A. and Galvin A.B. "Connecting speeds, Directions and
11. arrival times of 22 coronal mass ejections from the Sun the Sun to 1
12. AU", *J. Astrophys.*, pp. 119, 2014.
13. Owens M. and Cargill P. "Predictions of the arrival times of coronal mass ejections at 1AU: an analysis of the causes of the errors", *Ann. Geophys.*, 22, pp. 661-671, 2004.



14. Vrsnak B. and Gopalswamy N. "Influence aerodynamic drag on the motion of interplanetary ejecta", J. Geophys. Res., pp. 1019, 2002.
15. Akasofu S- I (1981) Energy coupling between the solar wind and the magneto- sphere. Space Sci Rev 28:121
16. 2 Astafyeva E, Yasyukevich U, Maksikov A, Zhivetiev I (2014) Geomagnetic storms, super- storms, and their impacts on GPS- based navigation sys- tems. Space Weather 12:508–525. doi:10.1002/2014SW001072
17. Echer E, Gonzalez WD (2004) Goeffectiveness of interplanetary shocks mag- netic clouds, sector boundary crossings and their combined occurrence. Geophys Res Lett. doi:10.1029/2003GL019199
18. Gonzalez WD, Joselyn JA, Kamide Y, Kroehl HW, Rostoker G, Tsurutani BT, Vasyliunas VM (1994) What is a geomagnetic storm? J Geophys Res 99(A4):5771–5792. doi:10.1029/93JA02867
19. Gopalswamy N, Akiyama S, Yashiro S, Xie H, Makela P, Michalek G (2015) The mild space weather in solar cycle. arXiv: 1508.01603.24
20. Hua L- N, Sonnerup BUO (1999) Two- dimensional coherent structures in the magnetopause: recovery of static equilibria from single- spacecraft data. J Geophys Res 104:6899–6918. doi:10.1029/1999JA900002
21. Kamide Y, Kusano K (2015) No major solar but the largest geomagnetic storm in the present solar cycle. Space Weather 13:365–367. doi:10.1002/2015SW001213
22. Kamide Y, Yokoyama N, Gonzalez W, Tsurutani BT, Daglis IA, Brekke A, Masuda S (1998) Two- step development of geomagnetic storms. J Geophys Res 103:6917–6922. doi:10.1029/97JA03337
23. Kataoka R, Shiota D, Keika E, Kilpua K (2015) Pileup accident hypothesis of magnetic storm on 17 March 2015. Geophys Res Lett 42:5155–5161. doi:10.1002/2015GL064816
24. Lakhina GS, Tsurutani BT (2016) Geomagnetic storms: historical perspective to modern view. Geosci Lett 3:5. doi:10.1186/s40562- 016- 0037- 4
25. Lepping RP, Burlaga LF, Johnes JA (1990) Magnetic field structure of interplan- etary magnetic clouds at 1 AU. J Geophys Res 95:11957. doi:10.1029/ JA095iA08p11957
26. Lepping RP, Berdichevsky D, Ferguson T (2003) Estimated errors in magnetic cloud model fit- parameters with force free cylindrically symmetric assumptions. J Geophys Res 108:1356. doi:10.1029/2002JA009657
27. Lepping RP, Wu C- C, Berdichevsky DB (2005) Automatic identification of mag- netic clouds and cloud- like regions at 1 AU: occurrence rate and other properties. Ann Geophys 23:2687–2704
28. Lepping RP, Berdichevsky DB, Wu C- C, Szabo A, Narock T, Mariani F, Lazarus AJ, Quivers AJ (2006) A summary of WIND magnetic clouds for years 1995–2003: model- fitted parameters, associated errors and classifications. Ann Geophys 24:215–245
29. Lepping RP, Wu CC, Berdichevsky DB, Szabo A (2015) Wind magnetic clouds for years 2010–2012: model parameter fittings, associated shock waves and comparisons to earlier periods. Sol Phys 290:2265–2290. doi:10.1007/s11207- 015- 0755- 3
30. Liu Y, Luhmann JG, Bale SD, Lin RP (2011) Solar source and heliospheric con- sequences of the 2010 April 3 coronal mass ejection: a comprehensive view. Astrophys J. doi:10.1088/0004- 637X/734/84
31. Liu YD, Hu H, Wang R, Yang Z, Zhu B, Liu YA, Luhmann JG, Richardson JD (2015) Plasma and magnetic field characteristics of solar coronal mass ejections in relation to geomagnetic storm intensity and variability. ApJL 809:1–6. doi:10.1088/2041- 8205/809/2/L34



34. Marubashi K, Cho KS (2015) Non- uniqueness of the geometry of interplan- etary magnetic flux ropes obtained from model- fitting. *Sun Geospace* 10:119–125
 35. McAllister AH, Crooker NU (1997) Coronal mass ejections, corotating interac- tion regions, and geomagnetic storms. In: Crooker N, Joselyn JA, Feyn- man J (eds) *Coronal mass ejections*. Geophysics monograph series, vol 99. AGU, Washington, D.C, pp 279–289. doi:10.1029/GM099p0279
 36. Möstl C, Farrugia CJ, Biernat HK, Leitner M, Kilpua EK, Galvin AB, Luhmann JG (2009) Optimized Grad–Shafranov reconstruction of a magnetic cloud using STEREO- Wind observations. *Sol Phys* 256:427–441. doi:10.1007/s11207- 009- 9360- 7
 37. Möstl C, Temmer M, Rollett T, Farrugia CJ, Liu Y, Vernoning AM, Leitner M, Galvin AB, Biernat HK (2010) STEREO and wind observations of a fast ICME flank triggering a prolonged geomagnetic storm on 5–7 April 2010. *Geophys Res Lett*. doi:10.1029/2010GL045175
 38. Ramsingh, Sripathi S, Sreekumar S, Banola S, Emperumal K, Tiwari P, Kumar BS (2015) Low- latitude ionosphere response to super geomagnetic storm of 17/18 March 2015: results from a chain of ground- based observations over Indian sector. *J Geophys Res* 120:10864–10882. doi:10.1002/2015JA021509
 39. Richardson IG, Cane H (2011) Geoeffectiveness (Dst and Kp) of interplanetary coronal mass ejections during 1995– 2009 and implications for storm forecasting. *Space Weather*. doi:10.1029/2011SW000670
- Tsurutani BT, Gonzalez WD (1997) The interplanetary causes of magnetic storms: a review. In: Tsurutani BT, Gonzalez WD, Kamide Y (eds) *Geophys- ics monograph series*, vol 98. American Geophysical Union, Washington, pp 77–89. doi:10.1029/GM098p0077